High-resolution multicomponent distributed acoustic sensing

Ivan Lim Chen Ning & Paul Sava, Center for Wave Phenomena, Colorado School of Mines

SUMMARY

The usage of Distributed Acoustic Sensing (DAS) in geophysics is attractive due to its dense spatial sampling and low operation cost if the optical fiber is easily accessible. In the borehole environment, optical fibers for DAS are often readily available as a part of other sensing tools, such as for temperature and pressure. Although the DAS system promises unlimited potential for reservoir monitoring and surface seismic acquisition, the single axial strain measurement of DAS along the fiber is inadequate to fully characterize the different wave modes, thus making reservoir characterization difficult. We propose a configuration using five equally spaced helical optical fibers and a straight optical fiber to obtain six different strain projections. This system allows us to reconstruct all components of the 3D strain tensor at any given location along the fiber. Using the condition number of the matrix product of the averaging and projection matrices, we can systematically search for the optimum design parameters for our configuration. Numerical examples demonstrate the effectiveness of our proposed method to successful reconstruction of the six component strain tensor from wavefields of arbitrary complexity.

INTRODUCTION

Despite the recent technological advances in DAS, multicomponent DAS remains a missing piece of the puzzle to capture the full character of the wavefield. In borehole application specifically, the usage of DAS focuses mainly on reservoir imaging (Mestayer et al., 2011; Mateeva et al., 2012, 2013; Wu et al., 2015; Zhan et al., 2015; Jiang et al., 2016) and velocity model updates (Wu et al., 2015; Li et al., 2015). Although, many examples show that DAS has the potential to provide low-cost reservoir monitoring (Hornman et al., 2015; Dou et al., 2016; Chalenski et al., 2016), the conventional single component DAS measurements makes reservoir characterization challenging. Moreover, a typical DAS system that employs Coherent Optical Time-Domain Reflectometry (COTDR) provides average strain measurement through analyzing the phase difference between two points along the optical fiber separated by a distance known as gauge length.

Since DAS acquires strain along the optical fiber, the measurement is a projection of the surrounding strain tensor as a function of the optical fiber position. Using multiple strain projections, it is possible to reconstruct the entire strain tensor; manipulating the geometry of the optical fiber allows us to obtain various strain projections. Lim and Sava (2016) provide a basic workflow on how multicomponent DAS can be recovered using dual optical fibers or a single chirping (variable pitch angle) helical optical fiber. The underlying principle of the workflow is to group consecutive strain measurements along optical fiber(s) within a defined window to perform the reconstruction. The drawback of this workflow is the assumption that the seismic wavelength is significantly larger than the specified window for successfully strain tensor reconstruction. A larger seismic wavelength than the window gives us a slowly varying strain tensor which we assume to be invariant within the window.

To overcome the limitation of the workflow introduced by Lim and Sava (2016), we propose a configuration with five equally spaced constant pitch angle helical optical fibers and a straight optical fiber. By doing so, we obtain six different strain projections at a given location to avoid the need to group consecutive strain measurements along optical fiber(s) to get sufficient strain projection for the reconstruction, thus overcoming the limitation of the workflow of Lim and Sava (2016). Six different strain projections at a given location can be done by using a configuration with five equally spaced constant pitch angle helical optical fibers, combined with a straight optical fiber. The configuration limits the engineering complexity required to build a multi-fiber cable, and also allows us to systematically analyze the effect of gauge length on strain tensor reconstruction. We reconstruct the strain tensor using the information of the strain projections $\mathbf{G}$ associated with the geometry of the optical fiber, and the gauge length captured in an operator $\mathbf{A}$ defined by the DAS system. Since we capture the effect of the gauge length, we remove the averaging effect in the reconstruction process, which allows us to use the reconstructed strain data as multicomponent geophone point measurements.

We demonstrate a systematic way to choose the helical optical fiber design parameters (diameter and pitch angle) and the gauge length characterizing our system by analyzing the condition number of the Gram matrix $\mathbf{L}^{\mathbf{T}}\mathbf{L}$ where $\mathbf{L} = \mathbf{AG}$. Using the chosen parameters, we reconstruct the full strain tensor through 3D synthetic examples of arbitrarily complex seismic wavefields (Figure 3d). This paper begins by reviewing the theoretical aspects of the proposed configuration, followed by 3D synthetic examples. While discussing the results, we also examine how the configuration parameters affect the reconstruction, by analyzing the associated condition number of the Gram matrix.

THEORY

DAS measures axial strain along the optical fiber, and therefore, it captures different projections of the surrounding strain tensor as a function of the location and geometry of the optical fiber. To describe the projec-

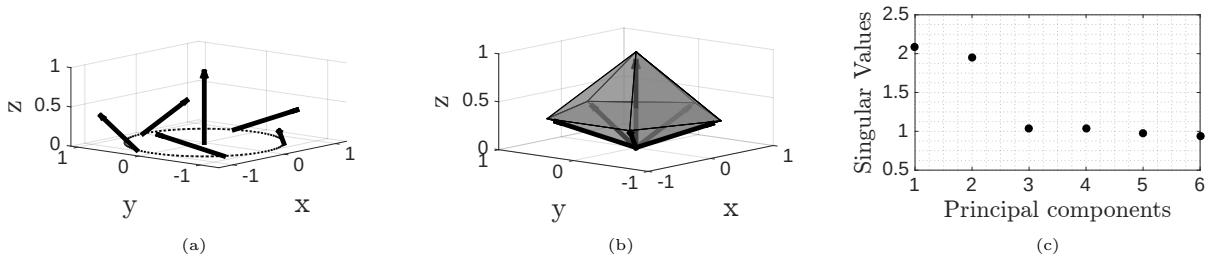

(a) (b) (c)

Figure 1: Fiber geometry with (a) five equally spaced vectors of 20° pitch angle and a straight vector in the middle. (b) Right pentagonal pyramid using the respective vectors in (a) and sharing the same origin. (c) The singular values of the corresponding Gram matrix.

tions, we use the intrinsic coordinate system of a curve as described by Pisano (1988) to express the local coordinate system of the optical fiber with respect to a global coordinate system. The tangent vector along the optical fiber is sufficient to relate the surrounding strain tensor to the axial strain measurement. The axial strain and the surrounding strain tensor can be related through the strain tensor coordinate transformation relationship as (Young and Budynas, 2002)

$$\bar{\boldsymbol{\varepsilon}} = \mathbf{R}\boldsymbol{\varepsilon}\mathbf{R}^{\mathbf{T}} \,, \tag{1}$$

where the $\bar{\boldsymbol{\varepsilon}}$ and $\mathbf{R}$ denote the transformed strain tensor and the transformation (also known as rotation) matrix respectively. We rearrange equation 3 as

$$\mathbf{b} = \mathbf{G}\mathbf{m} \,, \tag{2}$$

where $\mathbf{b}$ and $\mathbf{m}$ are the vectorized transformed and original strain tensor respectively. The matrix $\mathbf{G}$ is the expansion of equation 3 using the transformation matrix $\mathbf{R}$ and contains all the geometric information about the optical fiber. Using equation 2, the single optical fiber DAS measurement can be expressed as

$$\mathbf{d} = \mathbf{WAG}\mathbf{m} \,, \tag{3}$$

where $\mathbf{W}$ is an operator that defines the channel spacing (usually equal to the gauge length) which refers to the distance between consecutive average strain measurements within a gauge length, $\mathbf{A}$ is an operator describing strain averaging within a gauge-length, and $\mathbf{G}$ represents the projection operator which depends on the geometry of the system. At every single point along the optical fiber, we obtain the projected axial strain. An example of such operation is given as

$$\underset{\mathbf{b}}{\left[b_i\right]} = \underset{\mathbf{G}}{\begin{bmatrix} G_{xx,i} & G_{yy,i} & G_{zz,i} & G_{xy,i} & G_{xz,i} & G_{yz,i} \end{bmatrix}} \underset{\mathbf{m}}{\begin{bmatrix} \varepsilon_{xx,i} \\ \varepsilon_{yy,i} \\ \varepsilon_{zz,i} \\ \varepsilon_{xy,i} \\ \varepsilon_{xz,i} \\ \varepsilon_{yz,i} \end{bmatrix}} \,, \tag{4}$$

where the index i denotes points along the optical fiber. This process is repeated for every point along the optical fiber to produce the projected strain vector $\mathbf{b}$. We represent the combination operators of $\mathbf{WAG}$ as a linear operator $\mathbf{L}$, which allows us to reconstruct the strain tensor $\mathbf{m}$ in a least-squares sense as

$$\mathbf{m} = (\mathbf{L}^{\mathbf{T}}\mathbf{L})^{-\mathbf{1}}\mathbf{L}^{\mathbf{T}}\mathbf{d} \,. \tag{5}$$

To achieve accurate reconstruction using equation 5, the Gram matrix $\mathbf{L}^{\mathbf{T}}\mathbf{L}$ has to be invertible which is inferred from the condition number associated with its singular values. Therefore, it is advantageous to use the condition number as an indicator of strain tensor reconstruction capabilities. This also provides us with an opportunity to access various optical fiber system designs.

Lim and Sava (2016) perform the strain tensor reconstruction by grouping consecutive strain measurements along the optical fiber within a defined window. The grouping of consecutive measurements allows us to obtain a full rank Gram matrix for the strain tensor reconstruction. Their method requires as little as one optical fiber (a chirping helical optical fiber) to perform the reconstruction. However, this approach has the drawback that it assumes a seismic wavelength significantly larger than the reconstruction window. Our proposed configuration uses five equally spaced helical optical fibers with constant pitch angle. A constant pitch angle is less manufacturing challenging and allows us to obtain measurements at the same portion in space along all the helical optical fibers. We represent individual optical fibers in our proposed configuration with tangent vectors to conceptually visualize the associated measurements as shown in Figure 1a using a pitch angle of 20°. The lowest condition number is around 20°, for which we obtain sufficient horizontal and vertical strain projections to reconstruct all the strain components. The five equally spaced optical fibers provide enough azimuthal coverage for accurate strain reconstruction. Figure 1b shows that by using the same origin for all the vectors, we obtain a right pentagonal pyramid. Using the projection matrix $\mathbf{G}$ of the individual vectors, we evaluate the singular values of $\mathbf{G}^{\mathbf{T}}\mathbf{G}$ as shown in Figure 1c, which indicates that our configuration is full rank, as all the singular values are nonzero indicating that this configuration can reconstruct the entire strain tensor.

We analyze the effects of the gauge length $\mathbf{A}$ on our

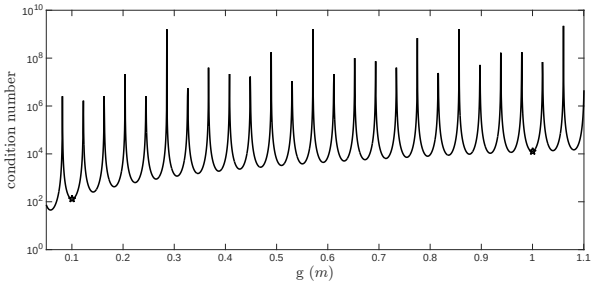

Figure 2: Condition number as a function of gauge length g using five helical optical fiber with diameter of 1 in and 20° pitch angle, and a straight optical fiber. The stars mark the condition number for gauge lengths of 0.1 and 1.0 m.

configuration by evaluating the condition number of the Gram matrix. Figure 2 illustrates the effect of gauge length between 0.05 and 1.10 m on the condition number of the Gram matrix for a cable with a diameter of 1 in and a pitch angle of 20°. We observe that there are many local minima (low condition number) throughout Figure 2 and the corresponding gauge lengths at the troughs of the graph are optimal for strain tensor reconstruction. For a gauge length of 1.0 m which corresponds to a trough, the condition number is in the order of 10^4 which implies that the reconstruction is likely to be significantly affected by noise. The oscillating characteristic of the condition number in Figure 2 shows that systematic reduction of the gauge length ensures a low condition number for high reconstruction accuracy.

NUMERICAL EXAMPLE

Using synthetic examples of a complex wavefield, we illustrate the reconstruction of the 3D strain tensor from axial strain measurements along the proposed optical fiber geometry using different gauge lengths. We simulate complex wavefields through triplications with a velocity model containing a low-velocity Gaussian anomaly, as shown in Figure 3c, using elastic finite-difference modeling. We use smaller than usual gauge lengths such as 0.1 m which are possible using specially designed optical fibers, as indicated by Farhadiroushan et al. (2016). However, we also perform the analysis using a gauge length of 1.0 m to show the effect of a more conventional fiber system.

Our experiment setup with a source indicated by a dot and receivers indicated by a straight line of coordinates (x_b, y_b) is shown in Figure 3a. Figure 3b, shown in a strain tensor matrix layout, represents our target strain tensor reconstruction observed along the receiver location at (x_b, y_b). The horizontal and vertical axes of the individual panels represent the reconstructed measurements along the optical fiber and time respectively. We perform the reconstruction by adding random noise with 30% of the maximum amplitude of the data and in the

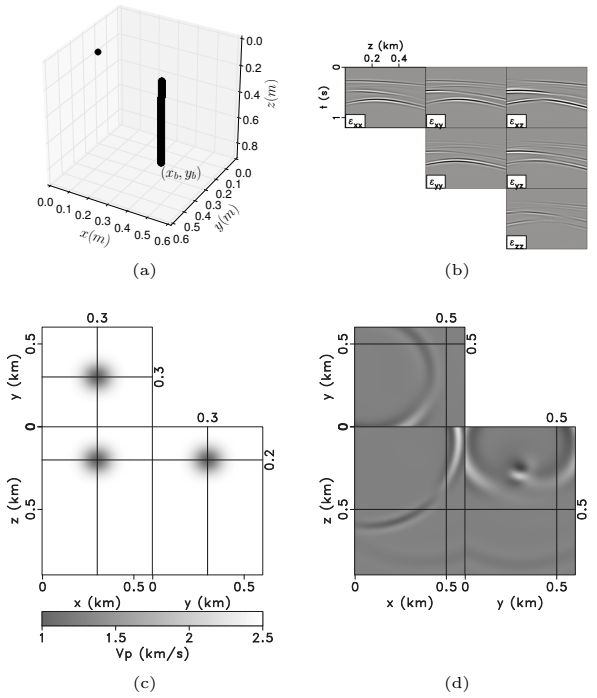

Figure 3: (a) Schematic representation of a DAS experiment depicting the source (dot) and receiver (line) locations. (b) The ideal strain tensor that we would like to reconstruct from DAS measurements. (c) The P-wave velocity model containing a low velocity Gaussian anomaly designed to produce wavefield triplications. The S-wave velocity is half of the P-wave velocity. (d) A snapshot of the vertical displacement wavefield.

data frequency band. Using a gauge length of 0.1 m, we can reconstruct the strain tensor as shown in Figure 4a. The difference plot in Figure 4b shows no signal leakage and only contain primarily random noise. Figure 4c shows the reconstruction results by increasing the gauge length to 1.0 m. We observe stronger arrivals although the results are noisy. The difference plot illustrated in Figure 4d contains noise primarily.

DISCUSSION

We demonstrate full strain tensor reconstruction with a high level of accuracy using six optical fibers (five equally spaced helical optical fiber with a pitch angle of 20° and a straight optical fiber). In our results, we show that by using a small but achievable gauge length with low condition number such as 0.1 m provides a robust strain tensor reconstruction due to the low condition number of the Gram matrix. A larger diameter of the helical configuration allows for a larger gauge length which improves the reconstruction results in noisier environments. A relaxed diameter dimension is more applicable for surface seismic acquisition. Using our proposed configuration, we can analyze the design parameters for the helical optical fibers systematically, as shown

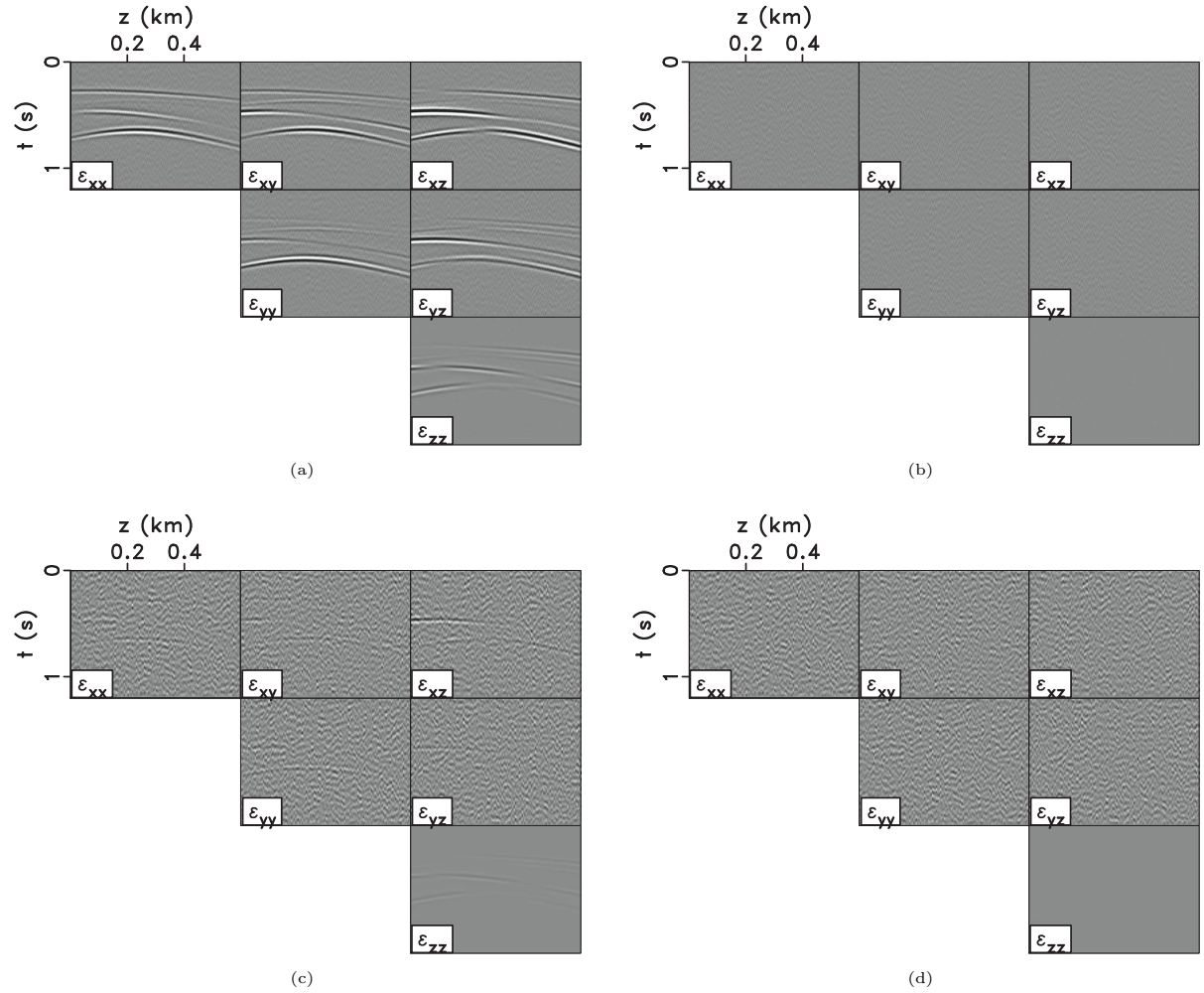

Figure 4: Strain tensor reconstructed from data containing random noise with 30% of the maximum data amplitude and band-limited to the data band with five equally spaced helical optical fibers and a straight optical fiber using a gauge length of (a) 0.1 and (c) 1.0 m. Panels (b) and (d) are the difference between the ideal strain tensor in Figure 3b and the respective reconstructed tensor in (a) and (c).

in Figure 2. The design goal is to obtain parameters that have the lowest possible condition number of the Gram matrix consist of the averaging **A** and projection matrix **G**, while also satisfying engineering constraints for optical fiber construction. Numerous configuration of equivalent robustness and quality are possible.

CONCLUSION

We demonstrate that high resolution multicomponent distributed acoustic sensing data is achievable by using strain projections along several optical fibers to reconstruct all components of the 3D strain tensor. Five equally spaced helical optical fibers, together with a straight optical fiber can be used for reconstruction without the need to group consecutive strain measurements along the optical fiber, within a defined window as shown by Lim and Sava (2016). We thus overcome the requirement that the seismic wavelength is significantly larger than the window and achieve high spatial resolution. This method opens the possibility for an acquisition of shorter seismic wavelengths, which aids imaging and reservoir characterization applications. Numerical examples show that our method can reconstruct the full 3D strain tensor for wavefields of arbitrary complexity, and in the presence of substantial noise in the band of the seismic data.

ACKNOWLEDGMENTS

We would like to thank the sponsors of the Center for Wave Phenomena, whose support made this research possible and Martin Karrenbach for fruitful discussions. The reproducible numeric examples in this paper use the Madagascar open-source software package (Fomel et al., 2013) freely available from http://www.ahay.org.

REFERENCES

Chalenski, D., M. Tatanova, Y. Du, A. Mateeva, J. Lopez, and H. Potters, 2016, Climbing the staircase of ultralow-cost 4D monitoring of deepwater fields using DAS-VSP, *in* SEG Technical Program Expanded Abstracts 2016: Society of Exploration Geophysicists, 5441–5445.

Dou, S., J. Ajo-Franklin, T. Daley, M. Robertson, T. Wood, B. Freifeld, R. Pevzner, J. Correa, K. Tertyshnikov, M. Urosevic, et al., 2016, Surface orbital vibrator (SOV) and fiber-optic DAS: Field demonstration of economical, continuous-land seismic time-lapse monitoring from the australian CO2CRC Otway site, *in* SEG Technical Program Expanded Abstracts 2016: Society of Exploration Geophysicists, 5552–5556.

Farhadiroushan, M., T. Parker, and S. Shatalin, 2016, Method and apparatus for optical sensing. (WO Patent App. PCT/GB2016/050,625).

Fomel, S., P. Sava, I. Vlad, Y. Liu, and V. Bashkardin, 2013, Madagascar: open-source software project for multidimensional data analysis and reproducible computational experiments: Journal of Open Research Software, **1**.

Hornman, J., A. Mateeva, J. Potters, and J. Lopez, 2015, New concepts for lowering the cost of frequent seismic reservoir monitoring onshore, *in* SEG Technical Program Expanded Abstracts 2015: Society of Exploration Geophysicists, 5518–5522.

Jiang, T., G. Zhan, T. Hance, S. Sugianto, S. Soulas, and E. Kjos, 2016, Valhall dual-well 3D DAS VSP field trial and imaging for active wells, *in* SEG Technical Program Expanded Abstracts 2016: Society of Exploration Geophysicists, 5582–5586.

Li, Y., H. Wu, W. Wong, B. Hewett, Z. Liu, A. Mateeva, and J. Lopez, 2015, Velocity analysis and update with 3D DAS-VSP to improve borehole/surface seismic images, *in* SEG Technical Program Expanded Abstracts 2015: Society of Exploration Geophysicists, 5285–5289.

Lim, I. C. N., and P. Sava, 2016, Multicomponent distributed acoustic sensing, *in* SEG Technical Program Expanded Abstracts 2016: Society of Exploration Geophysicists, 5597–5602.

Mateeva, A., J. Lopez, J. Mestayer, P. Wills, B. Cox, D. Kiyashchenko, Z. Yang, W. Berlang, R. Detomo, and S. Grandi, 2013, Distributed acoustic sensing for reservoir monitoring with VSP: The Leading Edge, **32**, 1278–1283.

Mateeva, A., J. Mestayer, B. Cox, D. Kiyashchenko, P. Wills, J. Lopez, S. Grandi, K. Hornman, P. Lumens, A. Franzen, et al., 2012, Advances in distributed acoustic sensing (DAS) for VSP: Presented at the 2012 SEG Annual Meeting, Society of Exploration Geophysicists.

Mestayer, J., B. Cox, P. Wills, D. Kiyashchenko, J. Lopez, M. Costello, S. Bourne, G. Ugueto, R. Lupton, G. Solano, et al., 2011, Field trials of distributed acoustic sensing for geophysical monitoring: Presented at the 2011 SEG Annual Meeting, Society of Exploration Geophysicists.

Pisano, A. P., 1988, The differential geometry of the general helix as applied to mechanical springs: Journal of Applied Mechanics, **55**, 831.

Wu, H., W.-F. Wong, Z. Yang, P. B. Wills, J. L. Lopez, Y. Li, B. Blonk, B. Hewett, and A. Mateeva, 2015, Dual-well 3D vertical seismic profile enabled by distributed acoustic sensing in deepwater Gulf of Mexico: Interpretation, **3**, SW11–SW25.

Young, W. C., and R. G. Budynas, 2002, Roark's formulas for stress and strain: McGraw-Hill New York, **7**.

Zhan, G., J. Kommedal, and J. Nahm, 2015, VSP field trials of distributed acoustic sensing in Trinidad and Gulf of Mexico, *in* SEG Technical Program Expanded Abstracts 2015: Society of Exploration Geophysicists, 5539–5543.